Index-Tunable Structured-Light Beams from a Laser with an Intracavity Astigmatic Mode Converter

Jing Pan,[1,2] Yijie Shen[3,*] Zhensong Wan,[1,2] Xing Fu,[1,2] Hengkang Zhang[1,2] and Qiang Liu[1,2,†]

[1]*Key Laboratory of Photonic Control Technology (Tsinghua University), Ministry of Education, Beijing 100084, China*

[2]*State Key Laboratory of Precision Measurement Technology and Instruments, Department of Precision Instrument, Tsinghua University, Beijing 100084, China*

[3]*Optoelectronics Research Centre, University of Southampton, Southampton SO17 1BJ, United Kingdom*

Structured-light lasers are highly topical due to not only their ability to tailor customized distribution of intensity, phase, orbital angular momentum (OAM), and other optical properties, but also the compact and simple at-the-source generation scheme. Here we propose a form of structured-light laser, intracavity mode convertor laser, with the ability to generate two-dimensional (2D) tunable high-order Hermite-Gaussian (HG) modes with a large indice range (up to 15). The mode convertor constituted by two cylindrical lenses is always used for external OAM conversion, but here we show that it can be inserted into a laser cavity as an intracavity element for symmetry-breaking control, which we also demonstrate with a complete matrix optics theory. The generated 2D HG modes can also be converted into Laguerre-Gaussian (LG) vortex beams with both tunable OAM and radial momentum. Moreover, we also show the ability to directly generate vortex beam from our laser cavity. Our approach meets the urgent necessity for a practical laser device for more versatile light, providing more alternative parametric space for structure control and fostering extended applications.

DOI: 10.1103/PhysRevApplied.14.044048

I. INTRODUCTION

In recent years, structured light, with the ability to arbitrarily tailor light in various optical properties such as intensity, phase, polarization, and orbital angular momentum (OAM), has risen in prominence [1]. In particular, it has been the emergence of vortex beams with tunable OAM [2], with the widespread applications in particle manipulation [3,4], high-security encryption [5], quantum entanglement [6], communications [7–9], nanophotonics mode excitation [10–13], and nonlinear optics [14–16]. Although a myriad of tools exist for structuring vortex beams external to the source [17–19], it is increasingly topical to directly create them from a laser cavity, namely structured-light lasers [20], which benefits both the improved purity of beam structures and the compactness of devices. Previous works have tried to insert special intracavity elements in the forms of spatial light modulators (SLM) [21], *q* plates [22], *J* plates [23], and other tailored metasurfaces [24,25] into a laser cavity for generating tunable OAM beams. However, as for SLM, it further requires complicated digital control device and

output power is limited by its low damage threshold, and also SLM is highly expensive. There also are bottlenecks for other insert elements: on one hand, the intracavity elements with artificial nanostructures are highly expensive to produce, on the other hand, the generated spatial modes cannot realize two-dimensional (2D) structured tunability, i.e., the mode indices both tunable at 2D transverse directions. Note that the 2D tunable mode would have great potential to extend applications of structured light. For example, a Laguerre-Gaussian (LG) mode $LG_{p,\ell}$, besides the well-known azimuthal index ℓ related to OAM, another independent index, radial index p, related to the radial momentum of light, is also recently applied in quantum entanglement [26], encoding information [27], and mode sorting [28]. Therefore, the vortex mode $LG_{p,\ell}$ with 2D tunable-mode indices (p, ℓ) reveals the full control of azimuthal and radial momenta of light, which can largely extend optical manipulation and related applications of structured light.

To generate a vortex beam, a classic and simple way is using a cylindrical lens pair as an astigmatic mode converter (AMC) to transform Hermite-Gaussian (HG) mode $HG_{m,n}$ into $LG_{p,\ell}$ beam with indices relationship of $p = \min(n, m)$ and $\ell = n - m$ [29–31]. With the AMC, the aim to generate a $LG_{p,\ell}$ is equivalent to generating a

---

HG$_{m,n}$, while the required HG modes can be generated by using off-axis pumping in a solid-state laser as an effective method [32–34]. However, in this way, only HG modes with one-dimensional tunable order can be generated directly from the cavity, because symmetry in one dimension only could be broken along the off-axis displacement of pumping, in other words, leading to the converted LG beams with tunable OAM but untunable radial index ($p = 0$) [31,34]. By inserting a 2D artificial mask into the cavity, a 2D high-order mode can be generated [35,36], but the fixed loss distribution prevents the mode indices from being freely tunable. In order to induce the tunable 2D symmetry breaking in the cavity, large-aperture pumping can be exploited for tunable 2D high-order mode [37–40], but the two indices in the two dimensions are coupled to each other, which could not realize independent 2D tunability. In short, it still urgently requires an effective and economic scheme to generate high-order modes with freely tunable 2D indices from a structured-light laser.

Here we propose a structured-light laser, which can controllably generate HG modes with 2D tunable indices directly from the cavity and 2D tunable vortex beams after mode conversion, and also has the ability to directly generate OAM beams. The approach is to insert an AMC, as an intracavity element, into a laser for tuning the 2D symmetry breaking in the cavity by controlling off-axis displacements of intracavity elements and pumping in two dimensions independently. We also propose a complete theoretical model based on matrix optics to demonstrate the 2D mode control effect, showing great agreement with the experimental results. This work offers a unique insight into the formation of tunable structured modes in laser cavities with a compact, simple, and cost-saving setup scheme, which has great potential to extend related applications such as optical tweezer, imaging, and communication.

II. EXPERIMENTAL SETUP DESIGN

The AMC has been widely utilized as an external modulator to perform the conversion between HG and LG modes. But here in our structured-light laser design, we apply the AMC as an intracavity element, which can impart a controlled 2D symmetry breaking of cavity including different beam characteristics, gain and loss in two dimensions, due to different curvature radii of intracavity AMC and off-axis control in two dimensions. Symmetry is broken in 2D by elaborately putting cylindrical lenses in an off-axis-pumped laser cavity. Off-axis of the cylindrical lens and pumping beam provides detuning to the cavity in two orthogonal directions, leading to dimension expending of generated HG modes. The output HG modes have tunable 2D indices controlled by the displacements of pump and the cylindrical lens, respectively. With AMC as the external converter of vortex beams,

modes carrying OAMs with continually and independently tunable azimuthal and radial indices (p, ℓ) are obtained.

The experimental setup is shown in Fig. 1. The pumping source is a 976-nm fiber-coupled laser diode, and the gain medium is an *a*-cut Yb:CALGO. A concave dichroic mirror and the output coupler form the cavity. Two cylindrical lenses ($F = 25$ mm both) inclined to 45° from the y' axis with the z axis as the rotation axis are set into the cavity as the control elements to stimulate a new tuning dimension
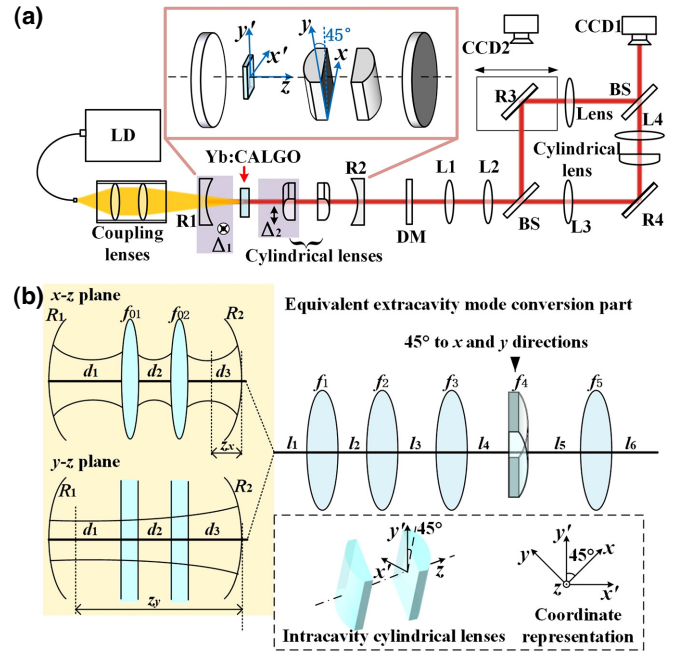

FIG. 1. Setup (a) in experiment with the insert showing the details of intracavity AMC structure, orientation of cylindrical lenses, definition of (x,y,z) and (x',y',z) coordinates [with the angle difference 45° between (x',y') and (x,y) coordinates, x' and y' axes along directions of two edges of Yb:CALGO section, respectively, the x axis and y axis perpendicular to and along generatrices of intracavity cylindrical lenses] and off-axis displacements of concave dichroic mirror R1 along the y' axis (Δ_1) and the first intracavity cylindrical lens along the x' axis (Δ_2), including the following: LD, laser diode (Han's TCS, highest power 110 W, with 105 μm fiber core and 0.22-NA numerical aperture); coupling lenses, 976-nm antireflective (AR) coated lenses [focal lengths (F): 30 and 60 mm]; Yb:CALGO ($4 \times 4 \times 2$ mm^3, 5 at.%, AR at 940–1080 nm); R1, concave dichroic mirror [AR at 979 nm and high reflective (HR) at 1040–1080 nm, radius of curvature: 1200 mm]; R2, output coupler (transmittance was 1% at 1030–1080 nm, radius of curvature: 300 mm); DM, dichroic mirror (reflectance is 99% at 979 nm and transmittance is 90% at 1050–1080 nm, filter off pumping light); lenses group, lenses L1 ($F = 25$ mm), L2 ($F = 30$ mm), and L3 ($F = 100$ mm), L4 ($F = 100$ mm); R3, R4, mirrors; BS, beam splitter (transmittance and reflectance both are 50% at 1064 nm); CCD, charge coupled device (Spiricon, M2-200s), with (b) equivalent light path including parameters in ABCD matrix theory and the insert of coordinate representation.

of modes. Cylindrical lenses are used for controlling the direction of HG modes along the cylindrical lenses' generatrix, and also for changing the HG mode's order of one dimension. Generated HG modes are converted into OAM beams through a group of lenses outside the cavity. The cylindrical lens ($F = 25$ mm) placed vertically is used for astigmatic conversion. We establish an interference system to check the topological charges of OAM beams. Reference light is led off by a beam splitter (BS) and expanded by a lens. OAM beams and the reference light converge through another BS to form the interference pattern, showing the topological charges of OAM beams.

III. THEORIES OF SYMMETRY-BREAKING MODES WITH INTRACAVITY AMC

The intracavity AMC breaks symmetry of the cavity, because the curvature radii of cylindrical lenses are different in two perpendicular directions (x direction perpendicular to and y direction along generatrices of intracavity cylindrical lenses). Different curvature radii have different effects on beam characteristics in two dimensions, such as radius of beam waist and Rayleigh length. Then corresponding gain and loss of the same order related with beam characteristics in two dimensions are different. The loss led in by R1 off axis along the y' axis has a large effect on the order along the x axis, and the loss led in by intracavity cylindrical lens off axis along the x' axis has a large effect on the order along the y axis. Moreover, different curvature radii of intracavity AMC also lead in special Gouy phase difference to two directions. Based on the above two points, corresponding 2D HG modes are selected, and after conversion, homologous 2D OAM modes are obtained. Thus orders are both tunable in two dimensions independently, and directions of two dimensions are dependent on the set intracavity AMC.

Besides mode indices tunable in two dimensions, intracavity AMC also incidentally introduces astigmatism into the cavity, which makes practical modes different from standard modes in the ellipticity of the transverse intensity profile. Thus, we use "OAM mode" distinguishing practical mode from standard LG mode. ABCD matrix optics theory is a suitable method to analyse astigmatism in practical modes. Practical beam characteristics can be obtained based on the matrix theory. With the practical beam characteristics in mode functions, astigmatic modes can be obtained in theory.

For the intracavity part, due to different beam characteristics in two dimensions caused by intracavity AMC, we combine the ABCD matrix and parameter q with HG function in different two dimensions to analyse output $HG_{m,n}$ modes. From the light path of the intracavity part shown in the experimental setup, intracavity AMC is the only symmetry-breaking element of the intracavity part and axes of two cylindrical lenses in the cavity are parallel

to each other. Thus two dimensions in the intracavity part are independent and ABCD matrices in the cavity of two dimensions can be treated separately [41–43]. One-round-trip ABCD matrices of the cavity perpendicular to ($\mathbf{X}$) and parallel with ($\mathbf{Y}$) the generatrices of cylindrical lenses are given as

$$\mathbf{X} = \mathbf{M}(d_3)\mathbf{N}\left(-\frac{1}{f_{02}}\right)\mathbf{M}(d_2)\mathbf{N}\left(-\frac{1}{f_{01}}\right)$$
$$\cdot \mathbf{M}(d_1)\mathbf{N}\left(-\frac{2}{R_1}\right)\mathbf{M}(d_1)\mathbf{N}\left(-\frac{1}{f_{01}}\right)$$
$$\cdot \mathbf{M}(d_2)\mathbf{N}\left(-\frac{1}{f_{02}}\right)\mathbf{M}(d_3)\mathbf{N}\left(-\frac{2}{R_2}\right), \qquad (1)$$

$$\mathbf{Y} = \mathbf{M}(d_3)\mathbf{M}(d_2)\mathbf{M}(d_1)\mathbf{N}\left(-\frac{2}{R_1}\right)$$
$$\cdot \mathbf{M}(d_1)\mathbf{M}(d_2)\mathbf{M}(d_3)\mathbf{N}\left(-\frac{2}{R_2}\right), \qquad (2)$$

where $\mathbf{M}(x) = \begin{bmatrix} 1 & x \\ 0 & 1 \end{bmatrix}$, $\mathbf{N}(x) = \begin{bmatrix} 1 & 0 \\ x & 1 \end{bmatrix}$, $\mathbf{X} = \begin{bmatrix} A_x & B_x \\ C_x & D_x \end{bmatrix}$, $\mathbf{Y} = \begin{bmatrix} A_y & B_y \\ C_y & D_y \end{bmatrix}$. d_1 to d_3 are distances between R1 and the first cylindrical lens, two cylindrical lenses, the second cylindrical lens and R2. R_1 and R_2 are curvature radii of R1 and R2. f_{01} and f_{02} are focal lengths of two cylindrical lenses, as Fig. 1(b).

Based on the relation between q_ξ (parameter q of beams in ξ direction at position Z_ξ, $\xi = x, y$) and the ABCD matrix in cavity $q_{\xi 1} = (A_\xi q_\xi + B_\xi)/(C_\xi q_\xi + D_\xi)$ (parameter $q_{\xi 1}$ is parameter q of beams in ξ direction at a new position $Z_{\xi 1}$ after transmission from the old position Z_ξ), and beam self-reproduction $q_{\xi 1} = q_\xi$, parameter $1/q_\xi$ can be expressed by the ABCD matrix as

$$\frac{1}{q_\xi} = \frac{D_\xi - A_\xi}{2B_\xi} - i\frac{1}{|B_\xi|}\sqrt{1 - \left(\frac{A_\xi + D_\xi}{2}\right)^2}. \qquad (3)$$

The imaginary part of complex parameter q_ξ is $q_{0\xi}$, and the real part of complex parameter q_ξ is the distance z_ξ away from beam waist, shown as

$$q_{0\xi} = \frac{i\frac{1}{|B_\xi|}\sqrt{1 - \left(\frac{A_\xi + D_\xi}{2}\right)^2}}{\left(\frac{D_\xi - A_\xi}{2B_\xi}\right)^2 + \frac{1}{|B_\xi|^2}\left[1 - \left(\frac{A_\xi + D_\xi}{2}\right)^2\right]},$$

$$z_\xi = \frac{\frac{D_\xi - A_\xi}{2B_\xi}}{\left(\frac{D_\xi - A_\xi}{2B_\xi}\right)^2 + \frac{1}{|B_\xi|^2}\left[1 - \left(\frac{A_\xi + D_\xi}{2}\right)^2\right]}.$$

$$(4)$$

Radius of beam waist $\omega_{0\xi}$ with the order ν is $\sqrt{2\nu + 1}$ times that of the fundamental mode. Based on the relation between $q_{0\xi}$ and radius of beam waist $\omega_{0\xi}$ and

Rayleigh length z_{R_ξ}, the radius of beam waist is $\omega_{0\xi} = \sqrt{-i(2\nu + 1)q_{0\xi}\lambda/\pi}$, and the Rayleigh length z_{R_ξ} is $z_{R_\xi} = \pi\omega_{0\xi}^2/\lambda$. Practical beam characteristics $\omega_{0\xi}$, z_{R_ξ} can be obtained by substituting $q_{0\xi}$ of Eq. (4).

HG mode solved from the Helmholtz equation with the order m along the x axis, the order n along the y axis is given by

$$\Psi_{m,n}^{(HG)}(x,y) = (2^{m+n-1}\pi m!n!)^{-1/2}\psi_m(x)\psi_n(y). \quad (5)$$

HG function in one dimension could yield ($\xi = x$, $\nu = m$; $\xi = y$, $\nu = n$)

$$\psi_\nu(\xi) = \frac{e^{-\xi^2/\omega_\xi^2(z_\xi)}}{\sqrt{\omega_\xi(z_\xi)}} H_\nu\left[\frac{\sqrt{2}\xi}{\omega_\xi(z_\xi)}\right] e^{ik[\xi^2/2R_\xi(z_\xi)]}$$
$$\times e^{-i(\nu+1/2)\tan^{-1}(z_\xi/z_{R_\xi})}, \quad (6)$$

where radius of beam $\omega_\xi(z_\xi) = \omega_{0\xi}\sqrt{1 + (z_\xi/z_{R_\xi})^2}$, and radius of equiphase surface $R_\xi(z_\xi) = z_\xi\left(1 + z_{R_\xi}^2/z_\xi^2\right)$ at z_ξ. By substituting beam characteristics $\omega_{0\xi}$, z_{R_ξ}, z_ξ obtained above to Eq. (5), actually acquired HG modes can be simulated.

Comparing with Fig. 2(a) the standard HG mode, by assigning $m = 3, n = 2$ in Eq. (5), HG modes directly from the cavity can be obtained in simulation as shown in Fig. 2(b), with $HG_{3,2}$ as an example. We find that besides the expansion of mode dimension, intracavity AMC also leads astigmatism into HG modes.

As for the extracavity mode conversion part, due to the external cylindrical lens set at 45° (extracavity cylindrical

lens rotated angle θ) to HG modes, it induces Gouy phase difference into two dimensions, converting HG modes into OAM modes. Different from the ABCD matrix analyzed independently in the cavity in two dimensions, the extracavity ABCD matrix of two dimensions cannot be treated independently, due to the cylindrical lens outside the cavity not being parallel with cylindrical lenses in the cavity. Therefore, an expansion matrix related to the extracavity cylindrical lens' angle of rotation is used to describe beam transmission outside the cavity, shown as

$$\mathbf{T} = \mathbf{P}(l_6, l_6)\mathbf{Q}\left(-\frac{1}{f_5}\right)\mathbf{P}(l_5, l_5)\mathbf{R}\left(\frac{1}{f_4}\right)$$
$$\cdot\mathbf{P}(l_4, l_4)\mathbf{Q}\left(-\frac{1}{f_3}\right)\mathbf{P}(l_3, l_3)\mathbf{Q}\left(-\frac{1}{f_2}\right)$$
$$\cdot\mathbf{P}(l_2, l_2)\mathbf{Q}\left(-\frac{1}{f_1}\right)\mathbf{P}(l_1 + z_x, l_1 + z_y), \quad (7)$$

where $\mathbf{P}(x,y) = \begin{bmatrix} 1 & 0 & x & 0 \\ 0 & 1 & 0 & y \\ 0 & 0 & 1 & 0 \\ 0 & 0 & 0 & 1 \end{bmatrix}$, $\mathbf{Q}(x) = \begin{bmatrix} 1 & 0 & 0 & 0 \\ 0 & 1 & 0 & 0 \\ x & 0 & 1 & 0 \\ 0 & x & 0 & 1 \end{bmatrix}$, $\mathbf{R}(x) = \begin{bmatrix} 1 & 0 & 0 & 0 \\ 0 & 1 & 0 & 0 \\ -x\cos^2\alpha & \frac{x\sin 2\alpha}{2} & 1 & 0 \\ \frac{x\sin 2\alpha}{2} & -x\sin^2\alpha & 0 & 1 \end{bmatrix}$ [44] related to rotated cylindrical lens with rotated angle $\alpha = 45°$. l_1 to l_6 are distances between R2, L1, L2, L3, cylindrical lens, L4 and CCD1 in turn. f_1 to f_3, and f_5 are focal lengths of L1 to L4, and f_4 is focal length of cylindrical lens. z_x and z_y are distances between R2 and corresponding beam waist of beam directly from the cavity based on Eq. (4), as Fig. 1(b).

With the extracavity ABCD expansion matrix in Eq. (7) and parameter $q_{0\xi}$ of modes directly from the cavity in Eq.
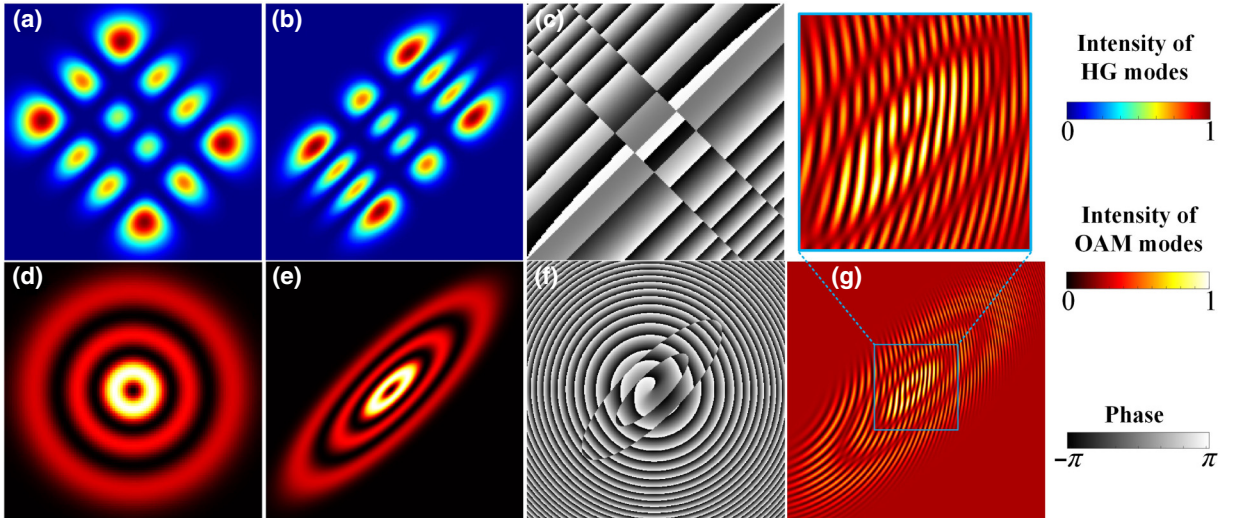

FIG. 2.   Simulated results of the structured laser beams: (a) standard $HG_{3,2}$ mode; (b) $HG_{3,2}$ mode directly from intracavity AMC laser and (c) its phase. (d) Standard $LG_{2,-1}$ mode. (e) $OAM_{2,-1}$ mode converted after intracavity AMC laser and (f) its phase. (g) The interference pattern of $OAM_{2,-1}$ mode and reference beam, the insert shows the enlarged figure of the coherent fringes.

(4), the relation between parameters q_ξ of beams after conversion and the extracavity ABCD expansion matrix are shown as

$$q_x = \frac{T_{11}q_{0x} + T_{13}}{T_{31}q_{0x} + T_{33}},$$
$$q_y = \frac{T_{22}q_{0y} + T_{24}}{T_{42}q_{0y} + T_{44}},$$ (8)

where $\mathbf{T}(i,j) = T_{ij}$. Beam characteristics are obtained with q_ξ in Eq. (8). The radius of beam waist is $\omega_{0\xi} = \sqrt{-iq_{0\xi}\lambda/\pi}$, where $q_{0\xi}$ is the imaginary part of q_ξ in Eq. (8), and the Rayleigh length z_{R_ξ} is $z_{R_\xi} = \pi\omega_{0\xi}^2/\lambda$. The real part of q_ξ in Eq. (8) is the distance z_ξ from corresponding beam waist.

Modes carrying OAMs after astigmatic conversion outside the cavity are written as [45,46]

$$\Psi^{(OAM)}\left(x',y'\right) = \sum_{s=0}^{N} d_{s-N/2,n-N/2}^{N/2}(\theta) \Psi_{s,N-s}^{(HG)}(x,y) e^{-is\beta},$$ (9)

where the elements of Wigner d matrix are given by

$$
\begin{aligned}
& d_{s-N/2,n-N/2}^{N/2}(\theta) \\
& = \sqrt{s!}\sqrt{(N-s)!}\sqrt{n!}\sqrt{(N-n)!} \\
& \times \sum_{v=\max[0,s-n]}^{\min[N-n,s]} \frac{(-1)^v [\cos(\theta)]^{m+s-2v} [\sin(\theta)]^{n-s+2v}}{v!\,(N-n-v)!\,(s-v)!\,(n-s+v)!}
\end{aligned}
$$ (10)

$N = n + m$, $x' = x\cos\theta + y\sin\theta$, $y' = x\sin(-\theta) + y\cos\theta$. Gouy phase difference of two dimensions $\beta = \pi/2 + \tan^{-1}(z_x/z_{R_x}) - \tan^{-1}(z_y/z_{R_y})$. By substituting practical beam characteristics $\omega_{0\xi}$, z_{R_ξ}, z_ξ based on Eqs. (8) to (9), OAM modes in the simulation can be obtained.

Comparing with Fig. 2(d), the standard LG mode, by assigning $m = 3$, $n = 2$ in Eq. (9), $OAM_{2,-1}$ converted from $HG_{3,2}$ shown in Fig. 2(e) is taken as an example.

The simulation deepens the understanding of astigmatic OAM modes, which are different from the standard LG modes in ellipticity of their transverse intensity profile, expanding the mode patterns as well as applications.

IV. EXPERIMENTAL RESULTS AND DISCUSSION

With experimental setup shown in Fig. 1, when all cavity elements are coaxial, fundamental mode is obtained at the pumping threshold of 0.56 W. With different off-axis displacements of intracavity cylindrical lens and R1, different loss and gain are brought in two dimensions, and output HG modes are selected as Fig. 3, recorded by CCD2 with R3 moved off. The specific relation between

obtained astigmatic HG modes $HG_{m,n}$ and different off-axis displacement of R1 along the y'-axis Δ_1, off-axis displacement of the first cylindrical lens along x'-axis Δ_2 and the pumping power P is shown as Table I in the Appendix. Modes like $HG_{0,i}$ ($i = 9 - 12, 14$), $HG_{1,i}$ ($i = 1,3$), $HG_{2,5}$, and $HG_{4,4}$ are also generated. However, for the case of very high-order modes (generally one index is larger than 10 or two indices both are not 0), due to the small difference of loss between two adjacent modes and the limitation of experimental adjustment accuracy of instrument, these modes can not be all stably captured, and thus we just show some relatively stable results as representatives.

From Fig. 3, HG modes can be controllably generated in two dimensions directly from the laser cavity. HG mode indices m and n are tunable continually and independently, changing with R1 off axis along the y' axis or one of the cylindrical lenses off axis along the x' axis, respectively. The varying range of m is from 0 to 4, and in total, output HG modes are in a large tunable range (more than 20 modes). The tunable range is limited by pumping power due to the relation between gain and loss, and with the increase of pumping power, tunable range enlarges. The output power of HG modes can be adjusted with pumping power, and with experimental pumping power, the output power is in milliwatt level. Moreover, shown as Fig. 3, the direction of HG modes is limited by the setting angle of the intracavity cylindrical lenses. Two dimensions are parallel to and perpendicular to the generatrix of intracavity AMC.

Generated certain $HG_{m,n}$ mode is converted into corresponding $OAM_{p,\ell}$ mode after mode conversion by going through the extracavity lens group (L1, L2, L3, cylindrical lens, and L4) as shown in the setup in Fig. 1. The
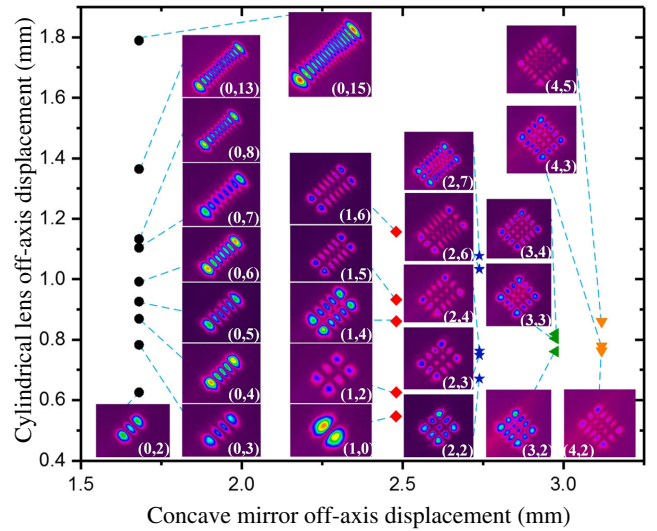

FIG. 3. Experimental results of the evolution of different generated HG modes with continually and independently tunable indices (m, n) with the off axis of the cylindrical lens and the concave mirror.
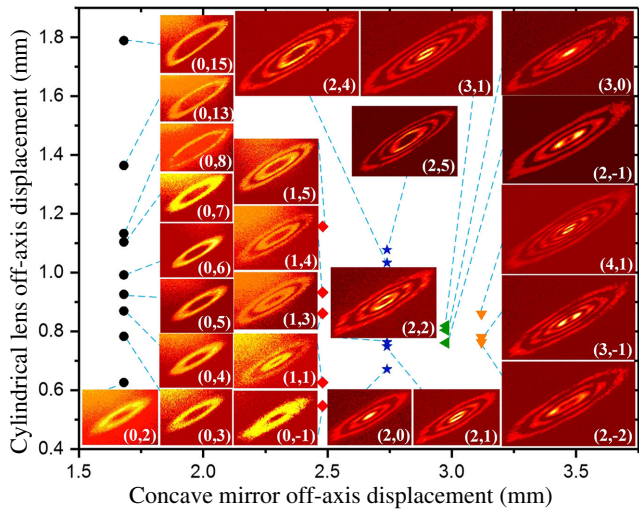
FIG. 4.   Experimental results of the evolution of different OAM modes carrying continually and independently tunable radial index and azimuthal index (p, ℓ) with the homologous off-axis displacements of the cylindrical lens and the concave mirror of HG modes.

radial index p is the smaller one of two parameters m and n, and the azimuthal index ℓ is n-m. Homologous OAM modes are recorded by CCD1, whose indices are stated specifically in Table I in the Appendix. In Fig. 4, OAM beams with continually and independently tunable radial and azimuthal indices (p, ℓ) are shown clearly. Limited by the generated HG modes, the tunable range of radial index

p is 0 to 4, and azimuthal index ℓ can be changed from -1 to 15, 0 to 5, -2 to 5, -1 to 1, 0 to 1, respectively. OAM modes' range can be changed with HG modes' tunable range.

Output power of OAM modes is also in milliwatt level with a high conversion efficiency from HG modes. Moreover, different from standard LG modes, output OAM modes are astigmatic obviously in Fig. 4, among which $OAM_{2,-1}$ is consistent with its simulational result in Fig. 2(e). Ellipticity in the transverse intensity profile of OAM modes in Fig. 4 is in the range of 0.19 to 0.28.

Angular momentum of OAM modes can be verified by interference patterns with reference beam. In our experiment, reference light is the flat part of the beam, which is led off by BS and expanded by the lens. Interference patterns are recorded by CCD1 as illustrated in Fig. 5. $OAM_{1,3}$, $OAM_{2,5}$, $OAM_{3,1}$, $OAM_{4,1}$ in Figs. 5(a1)–5(a4) are taken as examples for their different radial index p, with their interference patterns in Figs. 5(b1)–5(b4). The number of forks shows the topological charges three, five, one, one in each circle, respectively, corresponding to azimuthal index ℓ.

As an additional function of this cavity structure with the pair of cylindrical lenses set vertically in the cavity, OAM beams carrying $\pm 1\hbar$ can be generated directly from the cavity. Based on the light path above, the pair of cylindrical
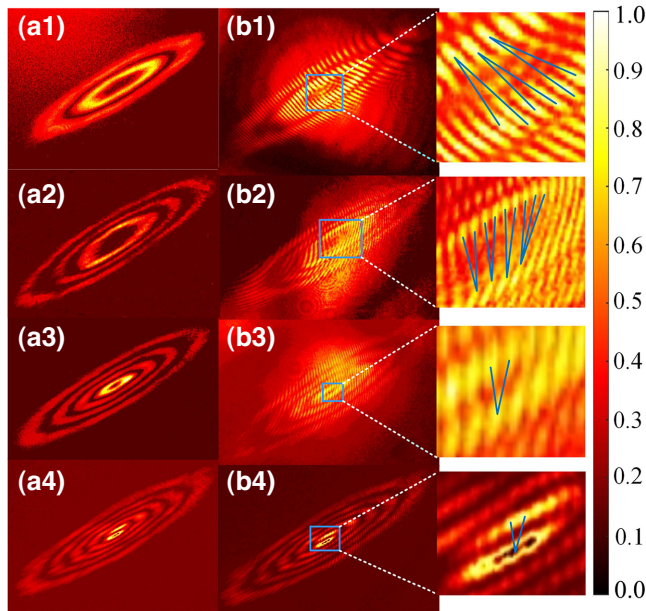

FIG. 5.   Experimental results of (a1–a4) $OAM_{1,3}$, $OAM_{2,5}$, $OAM_{3,1}$, $OAM_{4,1}$ and (b1–b4) corresponding interference patterns. The inserts show the enlarged figures of the coherent fringes in figures (b1–b4).
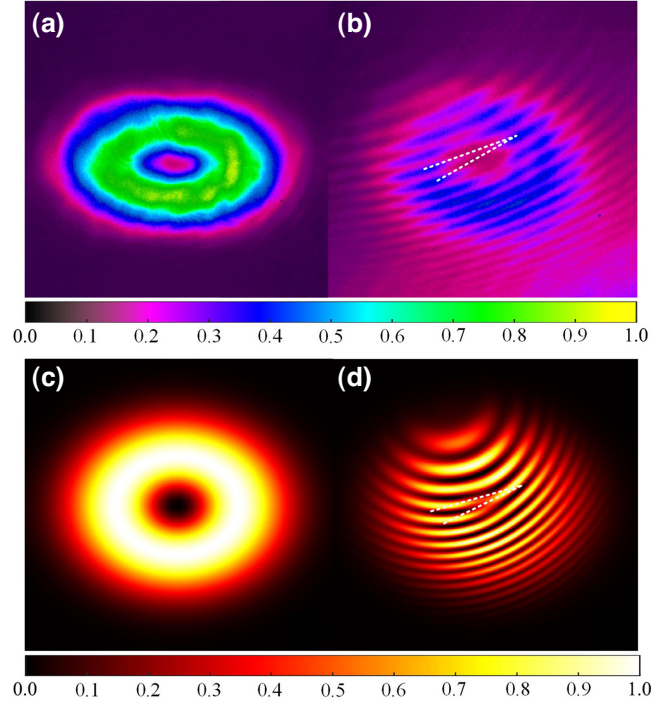

FIG. 6.   Experimental results of (a) $\pm 1\hbar$ OAM mode generated directly from the cavity and (b) the corresponding interference pattern. The simulated verifications of (c) the $\pm 1\hbar$ OAM mode and (d) the interference pattern.

TABLE I.   Pumping power and off-axis displacements for different HG modes and OAM modes.

$\Delta_1 = 1.681$ mm (round dots' row)				$\Delta_1 = 2.739$ mm (star dots' row)			
Δ_2(mm)	P(W)	$HG_{m,n}$	$OAM_{p,\ell}$	Δ_2(mm)	P(W)	$HG_{m,n}$	$OAM_{p,\ell}$
0.626	2.95	$HG_{0,2}$	$OAM_{0,2}$	0.671	5.49	$HG_{2,2}$	$OAM_{2,0}$
0.783	3.37	$HG_{0,3}$	$OAM_{0,3}$	0.749	6.06	$HG_{2,3}$	$OAM_{2,1}$
0.869	3.80	$HG_{0,4}$	$OAM_{0,4}$	0.763	6.16	$HG_{2,4}$	$OAM_{2,2}$
0.926	4.01	$HG_{0,5}$	$OAM_{0,5}$	1.033	7.93	$HG_{2,6}$	$OAM_{2,4}$
0.992	4.22	$HG_{0,6}$	$OAM_{0,6}$	1.077	8.69	$HG_{2,7}$	$OAM_{2,5}$
1.104	4.43	$HG_{0,7}$	$OAM_{0,7}$	$\Delta_1 = 2.975$ mm (regular triangle dots' row)			
1.133	4.43	$HG_{0,8}$	$OAM_{0,8}$	Δ_2(mm)	P(W)	$HG_{m,n}$	$OAM_{p,\ell}$
1.364	5.77	$HG_{0,13}$	$OAM_{0,13}$	0.761	7.80	$HG_{3,2}$	$OAM_{2,-1}$
1.789	7.41	$HG_{0,15}$	$OAM_{0,15}$	0.804	8.06	$HG_{3,3}$	$OAM_{3,0}$
$\Delta_1 = 2.480$ mm (diamond dots' row)				0.819	8.99	$HG_{3,4}$	$OAM_{3,1}$
Δ_2(mm)	P(W)	$HG_{m,n}$	$OAM_{p,\ell}$	$\Delta_1 = 3.119$ mm (inverted triangle dots' row)			
0.547	4.32	$HG_{1,0}$	$OAM_{0,-1}$	Δ_2(mm)	P(W)	$HG_{m,n}$	$OAM_{p,\ell}$
0.626	4.97	$HG_{1,2}$	$OAM_{1,1}$	0.763	8.83	$HG_{4,2}$	$OAM_{2,-2}$
0.861	5.86	$HG_{1,4}$	$OAM_{1,3}$	0.779	8.83	$HG_{4,3}$	$OAM_{3,-1}$
0.933	7.14	$HG_{1,5}$	$OAM_{1,4}$	0.860	10.03	$HG_{4,5}$	$OAM_{4,1}$
1.157	8.83	$HG_{1,6}$	$OAM_{1,5}$				

lenses are set 35.7 mm apart from each other between Yb:CALGO and R2. Δ_1 and Δ_2 are controlled as 0.847 mm and 0.068 mm, respectively, at the pumping power 4.01 W. Without the cylindrical lens outside the cavity, the mode is recorded by CCD1 shown in Fig. 6(a). Its interference pattern is recorded by CCD1 shown in Fig. 6(b). The number of forks shows the generated mode carrying $\pm 1\hbar$ OAM. Simulational result in Fig. 6(c) is obtained from Eq. (9) as $-1/f_4 = 0$ and $m = 0, n = 1$. For the case of generating 2D HG modes, the Gouy phase difference of beam between x, y directions is so small that only HG modes can be generated. While, for the case of generating OAM mode, we elaborately adjust the positions of the intracavity cylindrical lenses along the z axis, so that the Gouy phase difference between two orthogonal directions is nearly $\pi/2$, which allows the transformation from HG mode into OAM mode in cavity and the direct generation of OAM mode.

V. CONCLUSION

In conclusion, we use AMC as an intracavity element to construct a form of structured-light laser to generate 2D tunable high-order modes and vortex beams. In our approach, the 2D symmetry breaking is controllable by tuning off-axis displacements of intracavity AMC and cavity mirror, which leads to independent tunability of modes in 2D. A complete theoretical model combining the ABCD matrix and modal astigmatism is proposed to simulate the structured laser, which is well verified by experimental results. The generated $HG_{m,n}$ modes can be tuned continually and independently in two dimensions, with tunable indices up to 15. After external astigmatic conversion, OAM beams carrying continually and independently tunable radial and azimuthal indices (p, ℓ) are obtained, with a tunable range of p as 0 to 4, and that of ℓ from -2 to 15. It is the realization of vortex beam with both tunable orbital angular and radial momenta simultaneously. Additionally, $\pm 1\hbar$ OAM modes can be generated directly from the cavity by proper control. This work has great potential in increasing structured-light tunability at the source in a simple and cost-saving way, and providing deeper physical insight on understanding 2D practical astigmatic modes and enriching the related applications.

APPENDIX: TABLE OF OBTAINED MODES

HG modes and their converted OAM modes are shown in Table I with corresponding values of pumping power (P), off-axis displacement (Δ_1) of R1 and off-axis displacement (Δ_2) of the first intracavity cylindrical lens.

[1] H. Rubinsztein-Dunlop, A. Forbes, M. V. Berry, M. R. Dennis, D. L. Andrews, M. Mansuripur, C. Denz, C. Alpmann, P. Banzer, and T. Bauer *et al.*, Roadmap on structured light, J. Opt. **19,** 013001 (2016).

[2] Y. Shen, X. Wang, Z. Xie, C. Min, X. Fu, Q. Liu, M. Gong, and X. Yuan, Optical vortices 30 years on: OAM manipulation from topological charge to multiple singularities, Light: Sci. Appl. **8,** 1 (2019).

[3] M. Padgett and R. Bowman, Tweezers with a twist, Nat. Photonics **5**, 343 (2011).

[4] A. Lafong, W. J. Hossack, J. Arlt, T. J. Nowakowski, and N. D. Read, Time-multiplexed Laguerre-Gaussian holographic optical tweezers for biological applications, Opt. Express **14**, 3065 (2006).

[5] X. Fang, H. Ren, and M. Gu, Orbital angular momentum holography for high-security encryption, Nat. Photonics **14**, 102 (2020).

[6] A. Mair, A. Vaziri, G. Weihs, and A. Zeilinger, Entanglement of the orbital angular momentum states of photons, Nature **412**, 313 (2001).

[7] J. Wang, J.-Y. Yang, I. M. Fazal, N. Ahmed, Y. Yan, H. Huang, Y. Ren, Y. Yue, S. Dolinar, and M. Tur *et al.*, Terabit free-space data transmission employing orbital angular momentum multiplexing, Nat. Photonics **6**, 488 (2012).

[8] N. Bozinovic, Y. Yue, Y. Ren, M. Tur, P. Kristensen, H. Huang, A. E. Willner, and S. Ramachandran, Terabit-scale orbital angular momentum mode division multiplexing in fibers, Science **340**, 1545 (2013).

[9] J. Wang, Advances in communications using optical vortices, Photonics Res. **4**, B14 (2016).

[10] R. M. Kerber, J. M. Fitzgerald, X. Xiao, S. S. Oh, S. A. Maier, V. Giannini, and D. E. Reiter, Interaction of an Archimedean spiral structure with orbital angular momentum light, New J. Phys. **20**, 095005 (2018).

[11] G. F. Quinteiro and P. I. Tamborenea, Electronic transitions in disk-shaped quantum dots induced by twisted light, Phys. Rev. B **79**, 155450 (2009).

[12] R. M. Kerber, J. M. Fitzgerald, D. E. Reiter, S. S. Oh, and O. Hess, Reading the orbital angular momentum of light using plasmonic nanoantennas, ACS Photonics **4**, 891 (2017).

[13] Y. Meng, Z. Liu, Z. Xie, R. Wang, T. Qi, F. Hu, H. Kim, Q. Xiao, X. Fu, Q. Wu *et al.*, Versatile on-chip light coupling and (de) multiplexing from arbitrary polarizations to controlled waveguide modes using an integrated dielectric metasurface, Photonics Res. **8**, 564 (2020).

[14] L. Rego, K. M. Dorney, N. J. Brooks, Q. L. Nguyen, C.-T. Liao, J. San Román, D. E. Couch, A. Liu, E. Pisanty, and M. Lewenstein *et al.*, Generation of extreme-ultraviolet beams with time-varying orbital angular momentum, Science **364**, eaaw9486 (2019).

[15] K. M. Dorney, L. Rego, N. J. Brooks, J. San Román, C.-T. Liao, J. L. Ellis, D. Zusin, C. Gentry, Q. L. Nguyen, J. M. Shaw *et al.*, Controlling the polarization and vortex charge of attosecond high-harmonic beams via simultaneous spin-orbit momentum conservation, Nat. Photonics **13**, 123 (2019).

[16] C. Huang, C. Zhang, S. Xiao, Y. Wang, Y. Fan, Y. Liu, N. Zhang, G. Qu, H. Ji, J. Han *et al.*, Ultrafast control of vortex microlasers, Science **367**, 1018 (2020).

[17] W. Ji, C.-H. Lee, P. Chen, W. Hu, Y. Ming, L. Zhang, T.-H. Lin, V. Chigrinov, and Y.-Q. Lu, Meta-q-plate for complex beam shaping, Sci. Rep. **6**, 1 (2016).

[18] R. C. Devlin, A. Ambrosio, N. A. Rubin, J. P. B. Mueller, and F. Capasso, Arbitrary spin-to-orbital angular momentum conversion of light, Science **358**, 896 (2017).

[19] B. Piccirillo, V. D'Ambrosio, S. Slussarenko, L. Marrucci, and E. Santamato, Photon spin-to-orbital angular momentum conversion via an electrically tunable q-plate, Appl. Phys. Lett. **97**, 241104 (2010).

[20] A. Forbes, Structured light from lasers, Laser Photon. Rev. **13**, 1900140 (2019).

[21] S. Ngcobo, I. Litvin, L. Burger, and A. Forbes, A digital laser for on-demand laser modes, Nat. Commun. **4**, 1 (2013).

[22] D. Naidoo, F. S. Roux, A. Dudley, I. Litvin, B. Piccirillo, L. Marrucci, and A. Forbes, Controlled generation of higher-order poincaré sphere beams from a laser, Nat. Photonics **10**, 327 (2016).

[23] H. Sroor, Y.-W. Huang, B. Sephton, D. Naidoo, A. Vallés, V. Ginis, C.-W. Qiu, A. Ambrosio, F. Capasso, and A. Forbes, High-purity orbital angular momentum states from a visible metasurface laser, Nat. Photonics **14**, 498 (2020).

[24] E. Maguid, R. Chriki, M. Yannai, V. Kleiner, E. Hasman, A. A. Friesem, and N. Davidson, Topologically controlled intracavity laser modes based on Pancharatnam-Berry phase, ACS. Photonics **5**, 1817 (2018).

[25] E. Karimi, S. A. Schulz, I. De Leon, H. Qassim, J. Upham, and R. W. Boyd, Generating optical orbital angular momentum at visible wavelengths using a plasmonic metasurface, Light: Sci. Appl. **3**, e167 (2014).

[26] L. Chen, T. Ma, X. Qiu, D. Zhang, W. Zhang, and R. W. Boyd, Realization of the Einstein-Podolsky-Rosen Paradox Using Radial Position and Radial Momentum Variables, Phys. Rev. Lett. **123**, 060403 (2019).

[27] E. Karimi, R. W. Boyd, P. De La Hoz, H. De Guise, J. Řeháček, Z. Hradil, A. Aiello, G. Leuchs, and L. L. Sánchez-Soto, Radial quantum number of Laguerre-Gauss modes, Phys. Rev. A **89**, 063813 (2014).

[28] X. Gu, M. Krenn, M. Erhard, and A. Zeilinger, Gouy Phase Radial Mode Sorter for Light: Concepts and Experiments, Phys. Rev. Lett. **120**, 103601 (2018).

[29] L. Allen, M. W. Beijersbergen, R. J. C. Spreeuw, and J. P. Woerdman, Orbital angular momentum of light and the transformation of Laguerre-Gaussian laser modes, Phys. Rev. A **45**, 8185 (1992).

[30] M. W. Beijersbergen, L. Allen, H. E. L. O. Van der Veen, and J. P. Woerdman, Astigmatic laser mode converters and transfer of orbital angular momentum, Opt. Commun. **96**, 123 (1993).

[31] Y. Shen, Y. Meng, X. Fu, and M. Gong, Hybrid topological evolution of multi-singularity vortex beams: Generalized nature for Helical-Ince-Gaussian and Hermite-Laguerre-Gaussian modes, JOSA A **36**, 578 (2019).

[32] H. Laabs and B. Ozygus, Excitation of Hermite-Gaussian modes in end-pumped solid-state lasers via off-axis pumping, Opt. Laser Technol. **28**, 213 (1996).

[33] Y. F. Chen, T. M. Huang, C. F. Kao, C. L. Wang, and S. C. Wang, Generation of Hermite-Gaussian modes in fiber-coupled laser-diode end-pumped lasers, IEEE J. Quantum Electron. **33**, 1025 (1997).

[34] Y. Shen, Y. Meng, X. Fu, and M. Gong, Wavelength-tunable Hermite-Gaussian modes and an orbital-angular-momentum-tunable vortex beam in a dual-off-axis pumped Yb: CALGO laser, Opt. Lett. **43**, 291 (2018).

[35] S.-C. Chu, Y.-T. Chen, K.-F. Tsai, and K. Otsuka, Generation of high-order Hermite-Gaussian modes in end-pumped

solid-state lasers for square vortex array laser beam generation, Opt. Express **20**, 7128 (2012).

[36] W. Kong, A. Sugita, and T. Taira, Generation of Hermite-Gaussian modes and vortex arrays based on two-dimensional gain distribution controlled microchip laser, Opt. Lett. **37**, 2661 (2012).

[37] Y. Shen, Z. Wan, X. Fu, Q. Liu, and M. Gong, Vortex lattices with transverse-mode-locking states switching in a large-aperture off-axis-pumped solid-state laser, JOSA B **35**, 2940 (2018).

[38] Y. Shen, X. Yang, D. Naidoo, X. Fu, and A. Forbes, Structured ray-wave vector vortex beams in multiple degrees of freedom from a laser, Optica **7**, 820 (2020).

[39] Z. Zhang and C. Zhao, Spontaneous Phase and Frequency Locking of Transverse Modes in Different Orders, Phys. Rev. Appl. **13**, 024010 (2020).

[40] Z. Zhang and C. Zhao, Intra-cavity generation of linearly distributed and continuously varied optical vortices, IEEE Photonics Technol. Lett. **32**, 196 (2020).

[41] G. Nienhuis and S. J. M. Habraken, Structure of cavity modes with general astigmatism, Proc. SPIE 6483, Complex Light and Optical Forces 6483, 64830J (2007).

[42] S. J. M. Habraken and G. Nienhuis, Orbital angular momentum in twisted and rotating cavity modes, Proc. SPIE 6905, Complex Light and Optical Forces II 6905, 690504 (2008).

[43] S. J. M. Habraken and G. Nienhuis, Rotationally induced vortices in optical cavity modes, Journal of Optics A: Pure and Applied Optics **11**, 094006 (2009).

[44] A. E. Siegman, *Lasers University Science Books,* (Mill Valley, CA, 617, 1986).

[45] T. D. Huang and T. H. Lu, Large astigmatic laser cavity modes and astigmatic compensation, Appl. Phys. B **124**, 72 (2018).

[46] Y. F. Chen, C. C. Chang, C. Y. Lee, J. C. Tung, H. C. Liang, and K. F. Huang, Characterizing the propagation evolution of wave patterns and vortex structures in astigmatic transformations of Hermite-Gaussian beams, Laser Phys. **28**, 015002 (2017).